EPJ manuscript No.
(will be inserted by the editor)

The effects of Pt doping on the optical properties of Au_{20}

R. M. Jones[1], R. D'Agosta[2], and F. Baletto[3a]

[1] Physics Department, King's College London, WC2R 2LS, UK
[2] Nano-Bio Spectroscopy Group and European Theoretical Spectroscopy Facility, Departamento de Polìmeros y Materiales Avanzados: Fìsica, Quìmica y Tecnologia, Universidad del Pais Vasco, E-20018, San Sebastian, Spain and Ikerbasque, Basque Foundation for Science, Plaza de Euskadi 5, E-48009 Bilbao, Spain
[3] Physics Department, Universitá di Milano "La Statale", I-20133, Italy

Received: date / Revised version: date

Abstract. We consider the doping of Pt onto small Au_{20} clusters, identifying the effects that this alloying has upon the optical and static properties of each candidate nanoalloy. By performing real-time time dependent density functional theory calculations, we determine that the electronic structure and, by extension, the optical absorption spectrum strongly depend on the position of a Pt dopant; either as substitutional defect, or as an adsorbed atom on the Au-surface. Indeed, we find that by varying the chemical ordering, we are able to strongly influence the electronic and optical properties of complex nanoalloys. Of particular interest is the profound impact on the HOMO - LUMO gap of Au_{20} - shrinking or growing depending on the location of a Pt doping. By considering different possible locations and morphologies for the introduced Pt, we identify alloying types which may have a greater probability of supporting collective plasma oscillations.

PACS. 73.22.-f Electronic structure of nanoscale materials: clusters, nanoparticles, nanotubes, and nanocrystals – 73.61.At Metal and metallic alloys

1 Introduction

Metallic nanoalloys (NAs) have long been studied for their vast array of promising, novel applications, from biosensors to photovoltaics. Here, we are particularly interested in the optical properties of NAs, combining a plasmonic (gold) and a catalytic (platinum) material for their potential application in plasmon enhanced photo-catalysis [1,2]. Great attention has been paid to the development of such devices as the utilisation of localised surface plasmon resonances (LSPRs) has proven itself a viable and sustainable mean of generating kinetically active electrons and holes (hereafter collectively referred to as hot carriers) for photo-catalytic reactions [3–6]. Given current rising concerns as to the sustainability of current sources of energy production, it is critical to provide alternative means of generating and storing energy. It has been widely argued that molecular hydrogen, generated from water splitting, may be used for hydrogen fuel cells–an alternative to contemporary batteries.

To qualitatively understand the nature of the water splitting reaction on AuPt NAs, we look to recent experiments for our design philosophy [7–9], and adopt their principles of small Pt decorations upon a larger Au seed. This, in principle, ensures that the adsorption surface provided by the Pt is supported atop a larger Au nanoparticle (NP). The rationale behind this construction being that the Pt may be described as the 'fast' component of the cluster, whereas the Au as the 'hot'. Respectively, this is because Pt is known to be an excellent catalyst for the water splitting reaction [10]; and that Au has been demonstrated to have strong plasmonic behaviour at incident light wavelengths observed in solar output spectra [11,12].

Whilst it is common and reliable practice to consider many plasmonic effects from a classical perspective, such models assume a sharp cut-off at the boundary of the NP, in that all contained charges are bound by the surface. Indeed, this is often not the case: electron density can spill out, or tunneling effects between clusters can become effective [13]. As such, size dependent shifts of the main plasmon of isolated NPs or the existence of further surface collective modes that cannot be supported on stepped valence electron distributions are rendered unobtainable via classical models. However, for such nanometric systems, the dynamical many-body quantum mechanical description of LSPRs may be faithfully captured via time dependent density functional theory (TDDFT) methods. Within the domain of TDDFT, it is often unclear as to what the origin of an observed excitation may be. In one instance, it may indeed be the result of a collective oscilla-

[a] Email address: Robert.M.Jones@kcl.ac.uk, roberto.dagosta@ehu.es, francesca.baletto@unimi.it

tion of the metal's valence electrons, hence being correctly identified as a localised surface plasmon. However, it may also be the case that an observed peak in the absorption spectrum of a cluster is the result of a single electron - hole pair excitation. These are less desirable to generate in a cluster as they will typically recombine monotonically. Whereas we are instead interested in the Landau damping of an LSPR, which causes the collective oscillation to decay into a pair of hot carriers [6]. These hot carriers may then be directed from the catalytically active site into an adsorbed molecule. At the size scale considered, it is most likely that observed resonances will correspond to single-pair excitations [14] - especially in the case of Au_{20}^{Th} as the characteristically-large gap between the highest occupied molecular orbital (HOMO), and the lowest unoccupied molecular orbital (LUMO), makes the creation of continuous, and collective excitations prohibitively improbable.

Given the intrinsic quantum mechanical nature of such NAs, and the criticality of determining their plasmocatalytic properties, we have elected to perform a TDDFT study of small AuPt systems - closely monitoring their optical and static properties. It is our intention to demonstrate the profound relationship between the HOMO - LUMO gap, the a-periodic facsimile of the band gap; the distribution of electron orbital characters within the vicinity of the HOMO - LUMO region; and the computed photo-absorption and photo-emission spectra.

In this manuscript, we shall describe the computational methods employed, motivating their use given the context. In doing so, we shall demonstrate rich electrostatic, and electrodynamic properties of the nanoscale. We shall proceed to elucidate upon the aforementioned computed quantities, drawing conclusions from our results given the computed behaviour and physics known *a priori*. Finally, we shall present and justify our primary conclusion - that the complex interplay between morphology and chemical ordering in the alloyed phase will have profound consequences on the opto-electronic features of NAs which we strongly suspect is significant when considering a given NA's efficacy as a plasmocatalyst. We show that the HOMO - LUMO gap of two Au_{20} isomers can be finely tuned by displacing the Pt impurities as either a substitution or an adatom. By calculating the absorption spectra, in conjunction with the projected density of states (PDoS), we show clearly the importance of knowing the precise geometry when considering such complex NAs.

We acknowledge the extensive research conducted on the creation of metallic NAs through various doping processes for a variety of novel purposes, from enhanced catalytic properties [15,16] - to nurturing antimicrobial characteristics [17]. Moreover, we acknowledge the work of X. L. Lozano *et al* [18] in performing pioneering studies on the doping of similar Au structures with Ag to determine similar optical properties presented in this study. However, we are not aware of any literature relating Pt doping in Au nanostructures in the fashion we propose. As such, we believe that this work will help to develop a more fundamental understanding of larger nanostructures which are currently being investigated and deployed as plasmocatalysts [7].

This manuscript is organised as follows. In Section 2, the theoretical and computational details of the our investigation will be briefly introduced. This includes the diverse array of isomers and structures used as well as a qualitative description of our TDDFT prescription. Section 3 contains our results. A detailed analysis of the ground-state properties, and of the optical spectra with respect to the changes in geometry and chemical ordering. Finally, we compare in Section 4 the observed changes of the HOMO - LUMO gap, the PDoS, and the computed spectra at both the classical and quantum mechanical level of theory.

2 Methods

Our two initial structures of Au_{20} were a C1 point group symmetry (left column of Fig. 2) and the well-studied Tetrahedron (right column of fig. 2). The former low-symmetry structure can be created via single atom deposition upon the double-icosahedron structure with 19 atoms followed by a quench to an arbitrarily low temperature. We motivate our use of this structure in that many nanoparticles are flexible objects at finite temperature, and so to limit our considerations solely to high symmetry structures would be to willingly dismiss many structures which may very well be found to exist in laboratories. Moreover, we observe that it is not uncommon for nanoparticles to deform when subject to high intensity laser light. A process which may lead to the emergence of low symmetry nanoparticles and facets. Indeed, we have demonstrated in previous works how mechanical and optical properties are linked [19,20]. The latter is the energetically more favorable at this size, as confirmed by our calculations in agreement with the literature [21,22]. Our intention here being to simultaneously probe the effects of alloying on small Au clusters, and the effects that the seed morphology itself may have. For each system, we replace Au atoms from the initial structure with Pt, such that particle number was conserved. We have also adopted the approach of introducing the Pt defect as an ad-atom so as to better replicate, at a smaller scale, the design described in the work of Salmon *et al* [7]. We acknowledge the vast array of both high and low symmetry structures at the size scale we consider, however; we believe that this work may serve as a case-study from which further investigations into the structure - properties relationship may be performed.

We present in Fig. 1 structural discrepancies between the well-known Th structure, and the novel C1 isomer. We report the pair distance distribution function (PDF) which details the relative distance between pairs of atoms within the cluster. We may use this as a measure of amorphicity by considering the broadness and spread of the peaks. Moreover, we may use this to approximate the average first neighbour distance, r_0, by finding the location of the first minimum. We have also presented the distribution of atomic coordination numbers, this details the

type of local environments which may be found within the nanoparticle. We shall use these quantity to better elucidate on the structural properties of the NAs by computing the average coordination number, $\overline{NN}$, and the overage coordination of the introduced Pt, $\overline{NN_Pt}$ which will allow us to better appreciate the change in structure when developing the structure - properties relationship throughout the text.

We note the broader PDF curves on the left panel for the latter C1 nanoparticle (green curve) compared with the much finer PDF curve of the Th structure (black curve). We observe the reduction in the average first neighbour bond length in addition to profound changes in the distribution of the atomic coordination number. The latter of which demonstrates how much more compact the C1 cluster is relative to the Th. In the instance of the introduction of a Pt dopant via direct substitution, we selected the high symmetry site of tips, and lower symmetry sites of facets to introduce the defect as seen in Fig. 2. For introducing ad-atoms, we adsorbed Pt into hollow, and atop configurations. For each structure, we perform a classical geometry optimisation with the FIRE [23] algorithm as implemented in the atomic simulation environment (ase) and asap3 python packages [24,25], using inter-atomic potentials of the RGL form [26] with parameters provided by Baletto *et al.* [27]. We motivate the choice of classical potentials in the near equivalence of ground relaxed structures when computed via *ab initio* or classical methods. Hence, in the interest of minimising computational overheads, we elected to relax all structures with the FIRE algorithm. We note that the inclusion of Pt into the C1 structure led to noticeable structural rearrangement, particularly in the instance of doping.

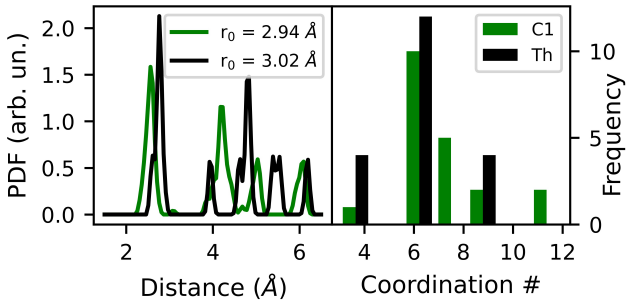

Fig. 1: Structural information comparing the pure structure considered in this study. Left panel is the PDF, and the right panel is the distribution of atomic coordination numbers. The insert reports the average first neighbour bond length, calculated the first minimum of the PDF.

From a classically optimised structure, we proceed to compute the ground state electronic density - recording its density of states (DoS), its atomic projected density of states (PDoS), and the HOMO - LUMO gap, ε_G. From a sufficiently well-converged ground state, we proceed to evolve each system in time by approximating the enforced time-reversal symmetry (AETRS) [28] to evaluate the time evolution operator. A time step of 0.33 attoseconds is used, and all systems are evolved for 16.5 fs.

To obtain optical and electronic properties at the quantum mechanical theory level, we have used the code of Octopus 11.1 [29,30] - a real-space DFT suite of codes designed for determining the spectroscopic details of finite systems via both linear response and real time propagation schemes. All of our calculations have been performed within the local density approximation (LDA) using norm-conserving pseudopotentials of the Hammann [31] and Troullier-Martins [32] types [33] which have permitted us to perform spin-polarised calculations to better capture the exotic phenomena presented by NAs. We have discretised the real space grid into cubic units of $(0.1\ \text{Å})^3$ which approximately corresponds to a plane-wave cutoff of 276.4 Ry. Our mesh is constructed by placing a sphere of radius 5 Å around each atom, constructed from a collection of grid units. To achieve better convergence of the ground state density, we smooth the Fermi-Dirac distribution with a cold smearing function [34] set to 1 meV. We remark that a small smearing was deemed necessary to reliably reach a sufficiently well converged ground state, especially with the inclusion of a Pt impurity. Furthermore, when a courser smearing of 10 meV was introduced, no perceptible difference was found with respect to the location of the HOMO and LUMO states.

A standard method of obtaining the absorption spectrum is via the quasi-static dipole approximation in that an instantaneous perturbation may be applied to the ground state density of the system at a time t_0 which takes the form,

$$\mathbf{E}(\mathbf{r},t) = K_0\delta(t)\mathbf{u} = \frac{1}{\pi}\int_0^\infty d\omega\ K_0\cos\omega t\mathbf{u}, \qquad (1)$$

essentially white light polarised along the vector $\mathbf{u}$ with incident intensity K_0. This perturbation results in an instantaneous transfer of momentum to the system which is then permitted to evolve under its own dynamics [35].

In principle, the optical absorption spectrum tensor may be directly calculated from the Fourier transform of the induced dipole moment, $\mathbf{d}(t) = \int \mathbf{r}\delta n(\mathbf{r},t)d\mathbf{r}$, with respect to time,

$$\hat{\sigma}_{\mathbf{u}}(\omega) = -\frac{\omega}{\pi K_0}\Im\int_0^\infty dt e^{(i\omega-\eta)t}\left(\mathbf{u}\otimes\mathbf{d}(t)\right), \qquad (2)$$

where η is some positive infinitesimal. We note that to obtain the optical spectrum, we need only know about the induced dipole density, and thus the induced electron density, $\delta n(\mathbf{r},t)$. The latter is the difference between the density at time t and at the initial time (usually that of the ground state) such that

$$\delta n(\mathbf{r},t) = n(\mathbf{r},t) - n(\mathbf{r},0). \qquad (3)$$

To compute the full polarisability tensor and, by extension the absorption spectrum, the dipole response must be calculated with respect to three spatially orthonormal vectors $\mathbf{u}$. Whenever the perturbation is sufficiently small,

the theory is equivalent to the standard linear response approach, based for example, on the Casida's equations [36] (see for instance, the user manual of Octopus for a comparison between the methods).

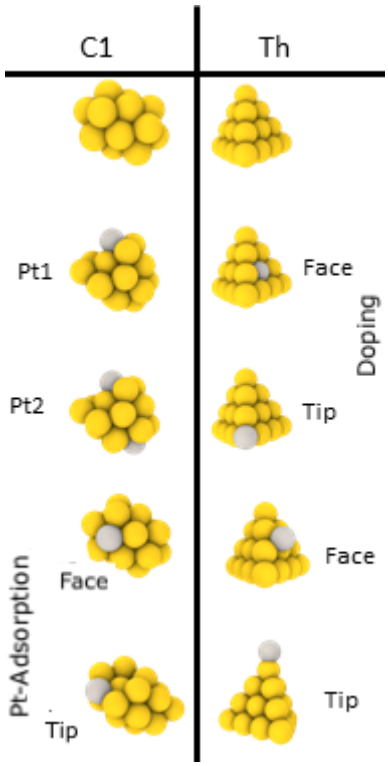

Fig. 2: Au_{20} isomers (row 1) considered for study. The subsequent two rows are doped structures, whilst the final two have ad-atoms.

3 Results

We first compute the ground state properties of the considered structures in Fig. 2. We monitor the changes to ε_G in Table 1 as the Au_{20}^{Th} is known to have a large HOMO - gap determined to be approximately 1.7 eV [37, 38]. We have determined this gap, with our $5d^{10}6s^1$ electronic configuration pseudopotential and within the LDA, to be 1.52 eV which is sufficiently representative of the physics of this cluster. Table 1 reports how altering the morphology and Pt loading of the cluster affects this fundamental feature of the NA. As found for other doping [38], the presence of Pt can both reduce or enlarge ε_G. We observe that, with the exception of the slight increase in HOMO- LUMO gap of Th-Dope-Tip by 30 meV, a more symmetric ionic structure may lead to a larger ε_G. As such, we find that by introducing Pt into low symmetry environments, we may reduce the size of the gap.

In considering Table 1, we note that there does not appear to be a general trend emerging between ε_G and the location, or indeed quantity, of the Pt. However, a curious property emerges for the Au_{20}^{Th} as an independent isomer. That being that the way in which we introduce Pt will influence strongly the closing of the gap. By adsorbing Pt onto the perfect structure, we are able to shrink the gap by approximately a factor of five. Conversely, if we simply perform the substitution, we observe no such influence on the gap.

Table 1: Effects of Pt doping of two isomers of Au_{20} on the HOMO - LUMO gap [eV], average first neighbour bond length, average atomic coordination number, and average Pt coordination where appropriate. All structures are ordered as they appear in Fig. 2.

Morph	Structure	ε_G [eV]	r_0 [Å]	$\overline{NN}$	$\overline{NN_{Pt}}$
Th	Pure	1.52	3.02	6.0	N/A
	Dope-Face	1.24	3.02	6.0	9.0
	Dope-Tip	1.55	3.02	6.0	3.0
	Adatom-Face	0.55	3.02	6.0	3.0
	Adatom-Tip	0.33	3.02	5.81	1.0
C1	Pure	0.03	2.94	7.2	N/A
	Dope-Pt_1	0.12	3.12	6.4	4.0
	Dope-Pt_2	0.58	3.07	6.4	5.0
	Adatom-Face	0.08	3.17	6.6	6.0
	Adatom-Tip	0.24	3.07	6.3	4.0

Alternatively, by considering the Au_{20}^{C1} structure, we actually observe the opposite behaviour. By introducing Pt to a low symmetry structure, we are able to open up a near non-existent gap. Indeed, when considering the lower left structures of Fig. 2, we see that geometrically relaxed structures arising from this isomer assume a vastly different conformation depending on the location and quantity of introduced Pt. Already, this disparity is in itself worthy of comment. A highly symmetric Au isomer remains structurally unperturbed, regardless of the method of Pt injection, whereas a low symmetry isomer is prone to disruption in the presence of a Pt dopant.

Moreover, by considering the geometrical properties presented in Table 1, we observe a considerable difference between how the Th and C1 structures accept introduced Pt. In the instance of the former, we see no appreciable change to the geometry as a consequence of introducing Pt either through doping or adsorption. Conversely, C1 demonstrates profound instability relative to its initial, unperturbed configuration. This is mostly evident in the rapid differences in the average first neighbour bond length, and the average atomic coordination number of the cluster.

In Figs. 3 and 4, we demonstrate the orbital characteristic, via the calculation of the atomic PDoS, of the electronic states up to the HOMO and for the following 10 unoccupied orbitals.In Octopus 11.1, the PDoS is computed from the bare pseudo-atomic orbitals, directly taken from the pseudopotentials we have used. The orbitals are not orthonormalised, in order to preserve the character of the atomic orbitals. Consequently, the sum of the different PDOS does not necessarily integrate to the total DoS. Hence the slight discrepancies observed in Figs. 3 and 4

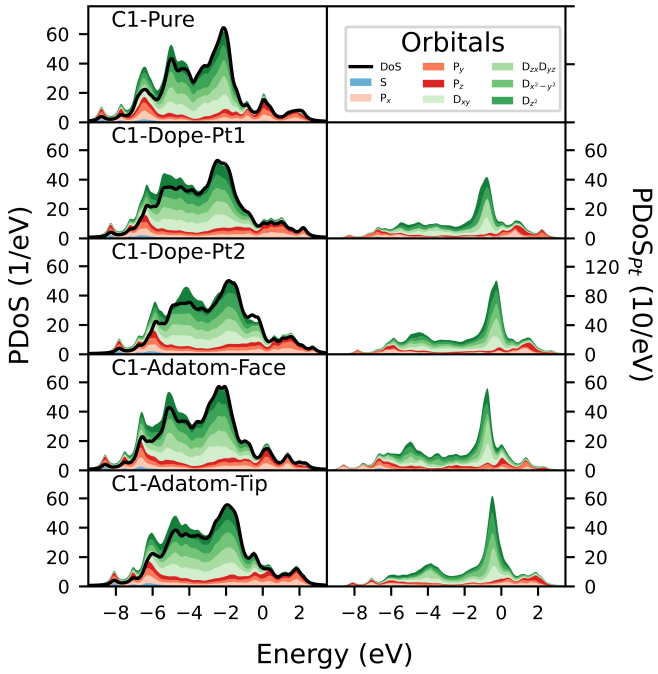

Fig. 3: Variation in the atomic projected density of states for the C1 candidate structures - left column of Fig. 2. Top left is for the pure structure only. Left panels illustrate the atomic PDoS for systems featuring Pt ordered as they appear in Fig. 2. Right panels present the atomic PDoS contributed from Pt only for their corresponding systems. Each plot has the total DoS presented as a black curve.

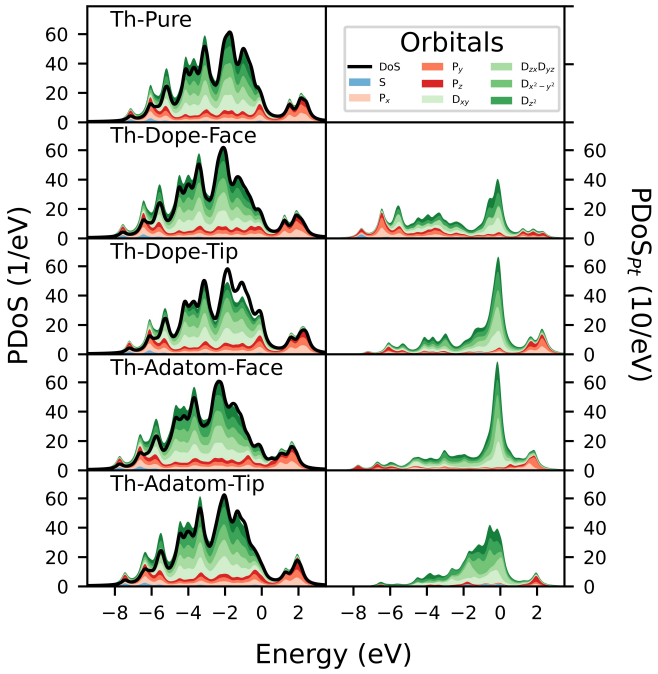

Fig. 4: Variation in the atomic projected density of states for the Th candidate structures - right column of Fig. 2. Top left is for the pure structure only. Left panels illustrate the atomic PDoS for systems featuring Pt ordered as they appear in Fig. 2. Right panels present the atomic PDoS contributed from Pt only for their corresponding systems. Each plot has the total DoS presented as a black curve.

between the reported DoS and PDoS. To create the figures, we have performed a Lorentzian broadening with a width of 217 meV around each of the Kohn-Sham eigenstates to smooth out the DoS, and to make interpretation of detail more facile. We are able to finely probe the nature of the HOMO - LUMO gap, as reported in Table 1, by considering nature of the atomic orbitals in the vicinity of these states. One might note that the LUMO has often a strong p-character. The nature of the HOMO orbital is more system-dependent but in several cases the HOMO is a combination of *pd*-type orbitals.

In Fig. 5, we present the absorption spectra as computed quantum mechanically via Eq. 2, averaging over the contributions from each of the orthonormal propagation vectors, $\sigma_{abs} = \mathrm{Tr}\hat{\sigma}_{\mathbf{u}}/3$. We note that for the reported wavelengths, we may consider our NAs to be sufficiently within the quasi-static approximation - reporting wavelengths upwards from 300 nm compared to an approximate NA size of 1 nm.

4 Discussion

By first evaluating the atomic PDoS of Figs. 3 and 4 with respect to the reported ε_G of Table 1, we note that not only does the gap strongly depend on the geometry and chemical composition of the structure, but so too does the characteristic of the orbitals which flank this gap. Indeed, this may account for some of the observed behaviour in the computed absorption spectra of Fig. 5 in that the introduction of Pt as an adatom on the tip may serve to enhance some modes at lower frequencies.

By considering the fundamental relationship between occupied and unoccupied states, and photo-absorption spectra we begin to identify potential optically active modes, which may have a plasmonic characteristic in origin even at the sub-nanometric scale. It is understood that optically active modes may be excited by either intraband transitions from the *d* to the *sp* orbitals, or by interband transitions within *sp* orbitals. In each case, the process must respect the conservation of angular momentum. Hence, we consider the distribution of orbital characteristics around the HOMO and LUMO as excitations are most likely to have their origin in states at and near to this region. There are strong *p* and *d* type orbitals near the HOMO - LUMO for all of the considered structures which suggests the existence of a rich array of angular momenta for the considered states. Moreover, by considering the right columns of Figs. 3 and 4, we see that the introduction of Pt has resulted in a strong delocalisation and hybridisation of states primarily centred at or near the HOMO. As such, excitations arising from the incidence of photons of a suitable frequency

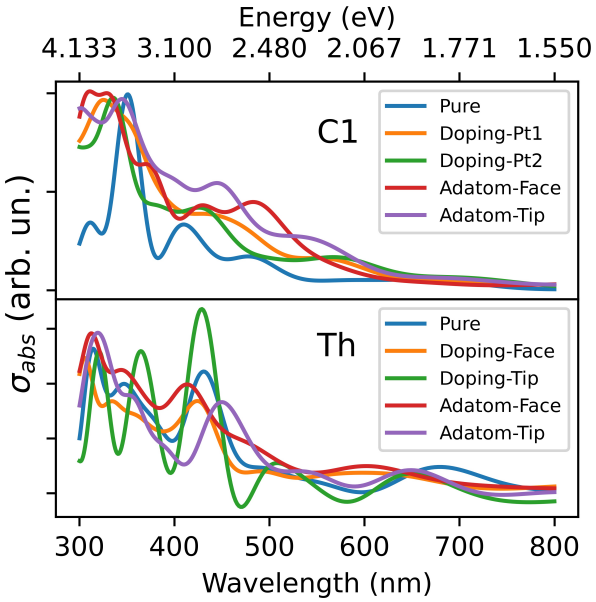

Fig. 5: Absorption and emission spectra of the Au_{20}^{C1} - upper - isomer and its derivative structures; and the Au_{20}^{Th} - lower - isomer and its derivative structures as computed via TDDFT methods.

have an increased likelihood of being localised at this Pt impurity. Indeed, this is precisely what is desirable, as the Pt has been described as an excellent catalyst for the water-splitting reaction. This reaction requires hot carriers as reagents. Hence, by having an increased propensity to localise hot carriers around Pt, is likely to improve the performance of a prospective plasmon-enhanced catalyst. This localising effect is seen most strongly in the less symmetric C1 structure, relative to the high symmetry of the Au tetrahedron. It is possible that this strong local character may arise from a lack of symmetry within the structure and will surely be a point of increased scholarly intrigue.

By monitoring the visualisation of the atomic PDoS relative to the HOMO - LUMO gap listed in Table 1, and comparing this information to the optical absorption spectra, seen in Fig. 5, we conclude that the lack of absorption at or around ε_G suggests that many of these modes are forbidden. Likely this is due to the necessary conservation of angular momentum being violated should an electron attempt to undergo such a transition. We note that multiple absorption peaks can be observed in the UV–vis–NIR absorption spectra for each considered structure, which may arise from single-electron transitions [39]. Indeed, the relative smoothness of the Au_{20}^{C1} and its derivative structures' spectra compared to those of the family of Au_{20}^{Th} suggests that the nature of a given excitation may be profoundly different between high and low symmetry NAs. We draw focus to the strong presence of peaks in the instance $Au_{19}^{Th}Pt_1^{Tip}$, whose gap was computed to be 1.55 eV, and observe the presence of three strong peaks (Fig. 5, green curve on the lower panel) in the UV-vis-NIR range. Compare this with Au_{20}^{C1}, whose gap is 50 times smaller at 0.03 eV and with a much smoother absorption spectrum in the same region with a visible peak at around 480 nm (Fig. 5, blue curve on the upper panel). This may well be indicative of an LSPR-like response to the perturbation.

Indeed, we note that not only does alloying strongly influence the character of the optical properties, indeed the morphology, even between pure Au clusters, has profound influences. Given our results, we believe that the core message is abundantly clear - the richness of new behaviour by the simple process of doping a small cluster with one or two Pt atoms will lead to the emergence of many alternative optically active modes with a strongly hybridised character of states localised within the neighbourhood of the dopant. In particular, a Pt on a tip configuration enhances the absorption independently of the Au-isomer. In short, the relative position of the dopant, not solely the relative amount, has been found to be responsible for changes in the optical properties, making crucial the monitoring of the chemical ordering in NAs. Indeed, this observation cannot only be constrained to the symmetry of the doping site; but rather, as our analyses have demonstrated, to the morphology of the initial structure itself, thus making clear the profound interplay between morphology, chemical ordering in the alloyed phase, and the opto-electronic features of NAs.

In this paper, we have demonstrated the strong influence that the introduction of Pt may have on the static and optical properties of small Au cluster. We have considered the characteristic of the orbitals in the region of the HOMO and the LUMO, in conjunction with the size of the gap and the presence of given optical modes. By studying these NAs at the level of TDDFT, we have been able to demonstrate how one may finely tune the optical properties, and even the localisation of potential hot carriers, by simply introducing Pt in a specific and targeted approach.

We hope this study will allow us to better understand how we may finely tune the optical and electronic characteristics of metallic NAs - not only for the purposes of plasmon enhanced photo-catalysis, but for the broader community of those working in the beautiful world of NAs.

Acknowledgements

This project is funded by Engineering and Physical Sciences Research Council. We thank HPC3 Europa, funded by the European Union's Horizon 2020 research and innovation programme under grant agreement No.730897, for computational resources on Mare Nostrum. Via our membership of the UK's HEC Materials Chemistry Consortium, which is funded by EPSRC (EP/L000202), this work used the UK Materials and Molecular Modelling Hub for computational resources, MMM Hub, which is partially funded by EPSRC (EP/P020194 and EP/T022213). This work used the ARCHER2 UK National Supercomputing Service (https://www.archer2.ac.uk). R.D'A. acknowledges support from the Grupos Consolidados UPV / EHU del Gobierno Vasco (Grant No. IT1249-19), the Red

Consolider of Spanish Government MINECO "TowTherm" (Grant No. ENE2017-90743-REDC) and Grant QuEST (Grant No. PID2020-112811GB-I00) funded by MCIN/AEI/10.13039/501100011033 and by "ERDF A way of making Europe" by the European Union. R. Jones and F. Baletto would like to thank Dr. Alejandro Santana-Bonilla for software development support. R. Jones acknowledges funding by the Engineering and Physical Sciences Research Council (EPSRC) through the Centre for Doctoral Training Cross-Disciplinary Approaches to Non-Equilibrium Systems (CANES, Grant No. EP/L015854/1).

Data availability statement

The data that support the findings of this study are available upon reasonable request from the authors.

5 Authors contributions

All the authors were involved in the preparation of the manuscript. All the authors have read and approved the final manuscript.

References

1. S. Mukherjee, L. Zhou, A. M. Goodman, N. Large, C. Ayala-Orozco, Y. Zhang, P. Nordlander, and N. J. Halas, "Hot-electron-induced dissociation of H_2 on gold nanoparticles supported on SiO_2," Journal of the American Chemical Society, vol. 136, no. 1, 2014.
2. S. Mukherjee, F. Libisch, N. Large, O. Neumann, L. V. Brown, J. Cheng, J. B. Lassiter, E. A. Carter, P. Nordlander, and N. J. Halas, "Hot electrons do the impossible: Plasmon-induced dissociation of H_2 on Au," Nano Letters, vol. 13, no. 1, 2013.
3. T. P. Rossi, P. Erhart, and M. Kuisma, "Hot-carrier generation in plasmonic nanoparticles: The importance of atomic structure," ACS Nano, vol. 14, no. 8, 2020.
4. V. Amendola, R. Pilot, M. Frasconi, O. M. Maragò, and M. A. Iatì, "Surface plasmon resonance in gold nanoparticles: a review," Journal of Physics: Condensed Matter, vol. 29, no. 20, 2017.
5. B. A. Prabowo, A. Purwidyantri, and K.-C. Liu, "Surface plasmon resonance optical sensor: A review on light source technology," Biosensors, vol. 8, no. 3, 2018.
6. V. G. Rao, U. Aslam, and S. Linic, "Chemical requirement for extracting energetic charge carriers from plasmonic metal nanoparticles to perform electron-transfer reactions," Journal of the American Chemical Society, vol. 141, no. 1, 2019.
7. J. U. Salmón-Gamboa, M. Romero-Gómez, D. J. Roth, M. J. Barber, P. Wang, S. M. Fairclough, M. E. Nasir, A. V. Krasavin, W. Dickson, and A. V. Zayats, "Optimizing hot carrier effects in pt-decorated plasmonic heterostructures," Faraday Discuss., vol. 214, 2019.
8. A. Y. Bykov, D. J. Roth, G. Sartorello, J. U. Salmón-Gamboa, and A. V. Zayats, "Dynamics of hot carriers in plasmonic heterostructures," Nanophotonics, vol. 10, no. 11, pp. 2929–2938, 2021.
9. J. U. Salmón-Gamboa, M. Romero-Gómez, D. J. Roth, A. V. Krasavin, P. Wang, W. Dickson, and A. V. Zayats, "Rational design of bimetallic photocatalysts based on plasmonically-derived hot carriers," Nanoscale Adv., vol. 3, pp. 767–780, 2021.
10. P. Lindgren, G. Kastlunger, and A. A. Peterson, "A challenge to the $G \sim 0$ interpretation of hydrogen evolution," ACS Catalysis, vol. 10, no. 1, 2020.
11. P. V. Kumar, T. P. Rossi, M. Kuisma, P. Erhart, and D. J. Norris, "Direct hot-carrier transfer in plasmonic catalysis," Faraday Discuss., vol. 214, 2019.
12. S. Linic, P. Christopher, and D. B. Ingram, "Plasmonic-metal nanostructures for efficient conversion of solar to chemical energy," Nature Materials, vol. 10, no. 12, 2011.
13. K. J. Savage, M. M. Hawkeye, R. Esteban, A. G. Borisov, J. Aizpurua, and J. J. Baumberg, "Revealing the quantum regime in tunnelling plasmonics," Nature, vol. 491, no. 7425, pp. 574–577, 2012.
14. M. Zhou, X. Du, H. Wang, and R. Jin, "The critical number of gold atoms for a metallic state nanocluster: Resolving a decades-long question," ACS Nano, vol. 15, no. 9, pp. 13980–13992, 2021. PMID: 34490772.
15. N. K. Chaki, H. Tsunoyama, Y. Negishi, H. Sakurai, and T. Tsukuda, "Effect of Ag-doping on the catalytic activity of polymer-stabilized Au clusters in aerobic oxidation of alcohol," The Journal of Physical Chemistry C, vol. 111, no. 13, pp. 4885–4888, 2007.
16. R. Jin, S. Zhao, C. Liu, M. Zhou, G. Panapitiya, Y. Xing, N. L. Rosi, J. P. Lewis, and R. Jin, "Controlling ag-doping in $Ag_xAu_{25-x}(SC6H11)_{18}$- nanoclusters: cryogenic optical, electronic and electrocatalytic properties," Nanoscale, vol. 9, pp. 19183–19190, 2017.
17. T. K. Pathak, R. Kroon, V. Craciun, M. Popa, M. Chifiriuc, and H. Swart, "Influence of ag, au and pd noble metals doping on structural, optical and antimicrobial properties of zinc oxide and titanium dioxide nanomaterials," Heliyon, vol. 5, no. 3, p. e01333, 2019.
18. X. López Lozano, C. Mottet, and H.-C. Weissker, "Effect of alloying on the optical properties of ag–au nanoparticles," The Journal of Physical Chemistry C, vol. 117, no. 6, pp. 3062–3068, 2013.
19. M. Vanzan, R. M. Jones, S. Corni, R. D'Agosta, and F. Baletto, "Exploring aurh nanoalloys: a computational perspective on the formation and physical properties," ChemPhysChem, vol. n/a, no. n/a, 2022.
20. W. Zhao, R. Jones, R. D'Agosta, and F. Baletto, "Making copper, silver and gold fullerene cages breathe," Journal of Physics: Condensed Matter, 2022.
21. M. Rapacioli, N. Tarrat, and F. Spiegelman, "Melting of the Au_{20} gold cluster: Does charge matter?," J. Phys. Chem. A, vol. 122, p. 4092–4098, 2018.
22. P. Gruene, D. M. Rayner, B. Redlich, A. F. G. van der Meer, G. Lyon, J. T.; Meijer, and A. Fielicke, "Structures of neutral Au_7, Au_{19}, and Au_{20} clusters in the gas phase," Science, vol. 321, pp. 674—-676, 2008.
23. E. Bitzek, P. Koskinen, F. Gähler, M. Moseler, and P. Gumbsch, "Structural relaxation made simple," Phys. Rev. Lett., vol. 97, p. 170201, Oct 2006.
24. A. H. Larsen, J. J. Mortensen, J. Blomqvist, I. E. Castelli, R. Christensen, M. Dułak, J. Friis, M. N. Groves, B. Hammer, C. Hargus, E. D. Hermes, P. C. Jennings, P. B. Jensen, J. Kermode, J. R. Kitchin, E. L. Kolsbjerg, J. Kubal, K. Kaasbjerg, S. Lysgaard, J. B. Maronsson,

T. Maxson, T. Olsen, L. Pastewka, A. Peterson, C. Rostgaard, J. Schiøtz, O. Schütt, M. Strange, K. S. Thygesen, T. Vegge, L. Vilhelmsen, M. Walter, Z. Zeng, and K. W. Jacobsen, "The atomic simulation environment—a python library for working with atoms," Journal of Physics: Condensed Matter, vol. 29, no. 27, p. 273002, 2017.
25. "asap3 software." `https://gitlab.com/asap/asap`.
26. V. Rosato, M. Guillope, and B. Legrand, "Thermodynamical and structural properties of f.c.c. transition metals using a simple tight-binding model," Philosophical Magazine A, vol. 59, no. 2, 1989.
27. F. Baletto, R. Ferrando, A. Fortunelli, F. Montalenti, and C. Mottet, "Crossover among structural motifs in transition and noble-metal clusters," The Journal of Chemical Physics, vol. 116, no. 9, pp. 3856–3863, 2002.
28. A. Castro, M. A. L. Marques, and A. Rubio, "Propagators for the time-dependent Kohn–Sham equations," The Journal of Chemical Physics, vol. 121, no. 8, pp. 3425–3433, 2004.
29. A. Castro, H. Appel, M. Oliveira, C. A. Rozzi, X. Andrade, F. Lorenzen, M. A. L. Marques, E. K. U. Gross, and A. Rubio, "octopus: a tool for the application of time-dependent density functional theory," physica status solidi (b), vol. 243, no. 11, 2006.
30. M. A. Marques, A. Castro, G. F. Bertsch, and A. Rubio, "octopus: a first-principles tool for excited electron–ion dynamics," Computer Physics Communications, vol. 151, no. 1, 2003.
31. D. R. Hamann, "Generalized norm-conserving pseudopotentials," Phys. Rev. B, vol. 40, pp. 2980–2987, Aug 1989.
32. N. Troullier and J. L. Martins, "Efficient pseudopotentials for plane-wave calculations," Phys. Rev. B, vol. 43, pp. 1993–2006, Jan 1991.
33. M. Fuchs and M. Scheffler, "Ab initio pseudopotentials for electronic structure calculations of poly-atomic systems using density-functional theory," Computer Physics Communications, vol. 119, no. 1, 1999.
34. N. Marzari, D. Vanderbilt, A. De Vita, and M. C. Payne, "Thermal contraction and disordering of the Al(110) surface," Phys. Rev. Lett., vol. 82, pp. 3296–3299, Apr 1999.
35. K. Yabana and G. F. Bertsch, "Time-dependent local-density approximation in real time," Phys. Rev. B, vol. 54, pp. 4484–4487, aug 1996.
36. M. E. Casida, Time-Dependent Density Functional Response Theory for Molecules in: Recent Advances in Density Functional Methods, Vol. 1 (D. P. Chong, Ed.). 01 1995.
37. Y. Gao, S. Bulusu, and X. C. Zeng, "Gold-caged metal clusters with large homo-lumo gap and high electron affinity," Journal of the American Chemical Society, vol. 127, no. 45, 2005.
38. F. Baletto and R. Ferrando, "Doped golden fullerene cages," Phys. Chem. Chem. Phys., vol. 17, pp. 28256–28261, 2015.
39. M. Zhou, T. Higaki, Y. Li, C. Zeng, Q. Li, M. Y. Sfeir, and R. Jin, "Three-stage evolution from nonscalable to scalable optical properties of thiolate-protected gold nanoclusters," Journal of the American Chemical Society, vol. 141, no. 50, pp. 19754–19764, 2019. PMID: 31809035.